Journal of
Materials Chemistry A

Materials for energy and sustainability
www.rsc.org/materialsA

Volume 1 | Number 1 | Jan 2013 | Pages 1–100

Journal of Materials Chemistry A

ARTICLE

Controllable assembly of two types of metal nanoparticles onto block copolymer nanospheres with ordered spatial distribution

S. Mei, J. Cao and Y. Lu

In this study, we report a novel method to assemble two types of metal nanoparticles onto poly(styrene-b-2-vinylpyridine) (PS-P2VP) block copolymer nanospheres with ordered spatial distribution. As a first step, core-shell metal-polymer particles have been fabricated, which consist of dodecanethiol (DT)-Au aggregation as core and PS-P2VP block copolymer as shell. Such core-shell particles have been obtained by swelling the DT-Au contained PS-P2VP nanoblocks, which are derived from Rayleigh instability of DT-Au@PS-P2VP nanotubes inside the cylindrical nanopores of anodic aluminum oxide (AAO) membranes. The core size and shell thickness of the particles can be tuned by the weight ratio of PS-P2VP to DT-Au content. An increase of the DT-Au content results in an increase of the DT-Au core size, combined with a red shift of the surface plasmon absorption peak in the UV-Vis spectra. Such core-shell particles have been further decorated with Pd nanoparticles on the shell due to the microphase separation of the PS-P2VP, which show efficient catalytic activity for the reduction of 4-nitrophenol by NaBH$_4$. Thus, the Au and Pd nanoparticles have been selectively assembled onto the PS-P2VP particles with ordered spatial distribution, leading to composite particles with multiple functions from both metal nanoparticles.

Introduction

The assemblies of metal nanoparticles with block copolymer (BCP) matrices have been intensively studied due to their various chemical compositions and ordered microphase structures.[1-7] They are considered as novel functional hybrid materials with applications in catalysis, sensors, optics and electronic devices.[8-11] The presence of well-ordered, high-content nanoparticles within BCP matrices offers the hybrid materials with enhanced collective properties, which do not present in their individual state.[12] For example, the assembly of plasmonic nanoparticles into secondary structures may create "hot spots" for surface-enhanced Raman scattering (SERS) due to the plasmon coupling between adjacent particles.[13] Until now, different strategies have been developed for target-loading metal nanoparticles to BCP nanostructures, including solution precipitation,[14-16] interfacial instabilities of emulsion droplets,[17] heating-cooling processing,[18] and directed supramolecular assembly.[19] For instance, Kim and co-workers[20] have synthesized BCP microspheres with Au cores from an evaporative toluene-in-water emulsion in which polystyrene-b-poly(4-vinylpyridine) (PS-P4VP) incorporated with Au precursors (AuCl$_4^-$) are dissolved in toluene. Jin et al.[21] reported the patterned decoration of gold nanoparticles on the surface of poly(styrene-b-2-vinylpyridine) (PS-P2VP) particles

using in situ reduction of HAuCl$_4$ in P2VP domains under UV irradiation. However, until now most works of this sort focus on the assembly of one single metal nanoparticles,[22-24] few experiment has been conducted on the assembly of two different types of metal nanoparticles to BCP particles with ordered spatial distribution. In addition, it is still a challenge to prepare hybrid particles with sufficient amount of metal nanoparticles for practical device applications. Usually the interaction between the high-content metal nanoparticles and their favorable block of the BCP will increase its effective volume, resulting in changes of the microphase separation structure. In general, it is critical to control both the distribution and sufficient loading of metal nanoparticles within the BCP particles.

Among the widely used assembly methods, the newly explored strategy based on the Rayleigh instability of polymer nanotubes confined in anodic aluminum oxide (AAO) nanopores[25] has attracted lots of interests. The underlying physical chemistry between the AAO wall and the injected materials[26] provides potential applications for the fabrication of novel composite nanoparticles. AAO has been widely used as template for the fabrication of one-dimensional (1D) nanostructures, such as nanotubes and nanorods.[27-32] Rayleigh instability is used to describe the undulating phenomenon of liquid cylinders due to surface tension.[33]
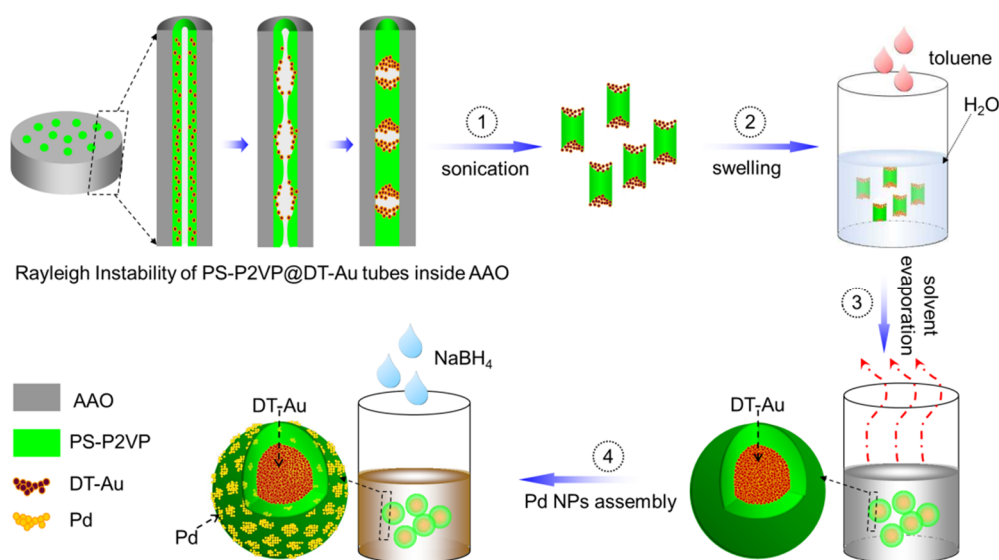
Scheme 1. Procedure of the preparation of Pd@DT-Au@PS-P2VP particles based on Rayleigh instability phenomenon of hybrid nanotubes in AAO capillary channels. (1) Dissolving of AAO template by NaOH and cutting the nanorods into short segments through ultrasonication. (2) Swelling by toluene. (3) Evaporation of toluene. (4) Surface decoration of the core-shell particles with Pd nanoparticles.

In 2007, Russell et al.[34-35] firstly realized the experimental study about Rayleigh instability of polymer nanotubes confined in AAO nanopores. With the undulation of polymer nanotubes, crests merged to form bridges across the AAO pores, nanorods with periodic encapsulated holes were obtained. Based on this phenomena, Jin et al.[25] explored a novel method for the fabrication of size tunable polymer particles by swelling the short rodlike entities generated from Rayleigh instability of polymer nanotubes inside the AAO nanopores. In consideration of the interactions of the AAO wall with different injected materials, this strategy also provides possibilities for the generation of phase separated metal-nanoparticles@BCP hybrid nanostructures, which can be promising candidates for the fabrication of BCP particles loaded with different types of metal nanoparticles. In addition, the AAO method allows the application of commercial block copolymers with narrow polydispersity index (PDI), which is crucial for the generation of ordered microphase separation structures.

Herein, we report a novel approach for the fabrication of well-ordered metal@BCP particles selectively loaded with two types of metal nanoparticles. Scheme 1 illustrates the fabricating procedure. Pre-synthesized Au nanoparticles capped by DT molecules were first mixed with PS-P2VP and injected into AAO nanopores to fabricate metal-polymer hybrid tubes. A thermal annealing is applied to induce the phase separated structures of the hybrid nanorods. These nanorods are then cut into small segments through ultrasonication, followed by a swelling process to transform the short nanorods to nanospheres. In order to study the influence of the DT-Au content on the morphology of the products, different amounts of DT-Au nanoparticles are used. The optical properties of such composite particles are tested by UV-Vis spectrometer. The patterned P2VP domains on the shell have the ability to form complexes with various metal ions. In the present study, in situ reduction of the $PdCl_4^{2-}$ ions anchored in the P2VP domains leads to the assembly of Pd nanoparticles into the system. The catalytic activity of the DT-Au@PS-P2VP particles before and after Pd deposition has been studied. To the best of our

knowledge, this is the first report on the assembly of two different types of metals to BCP particles with well-ordered spatial distribution, which will provide an opportunity to utilize the unique properties of different metal nanoparticles, thus broads their potential applications in high-performance catalysis, bioengineering and medical therapy.[36-38]

Experimental

Chemicals and Materials

Poly(styrene-b-2-vinylpyridine) (PS-P2VP) (Mn (PS) = 50000 g/mol; Mn (P2VP) = 16500 g/mol; Mw/Mn = 1.06) was obtained from Polymer Source Inc. Sodium dodecyl sulfate (SDS), dodecanethiol (DT), HAuCl₄•3H2O, tetraoctylammonium bromide (TOBA), 4-nitrophenol, analytical grade toluene, ethanol, sodium hydroxide and sodium borohydride were purchased from Sigma Aldrich, and used as received. De-ionized water was used for all aqueous solutions. Anodic aluminum oxide (AAO) membranes (Anodisc 13, 0.2 μm) were purchased from Whatman Ltd. The membranes were rinsed thoroughly with dichloromethane, tetrahydrofuran, and de-ionized water in sequence and then dried in vacuum before use.

Preparation of DT-Au nanoparticles

DT-Au nanoparticles were prepared following the Brust two-phase reaction procedure.[39] A HAuCl₄•3H2O (0.6 mmol) aqueous solution (60 mL) was added to tetraoctylammonium bromide (TOAB, 1.2 mmol) dissolved in toluene (160 mL). Under vigorously stirring, the yellow aqueous solution became colorless, and the toluene phase turned orange as a result of the complexing of [AuCl₄]- with tetraoctylammonium cations. The above solution was mixed with DT (0.6 mmol) in toluene (20 mL) for 10 min at room temperature. A freshly prepared aqueous solution (60 mL) of sodium borohydride (6 mmol) was added to the vigorously stirred mixture. After 12 hrs' stirring, the obtained Au nanoparticles were separated by centrifugation

(8000 rpm, 60 min), removal of the supernatant. The precipitation was cleaned by ethanol for three times. The product was dissolved in 30 mL toluene for the further preparation of DT-Au@PS-P2VP wetting solution.

Fabrication of DT-Au@PS-P2VP core-shell particles

For the wetting of the AAO membrane, one drop of DT-Au@PS-P2VP/toluene solution (5 μl) was placed on a glass slide. Subsequently, an AAO membrane was placed on the top of the solution. The nanopores of the membrane were filled with such mixed solution within seconds by capillary force. The membrane was first dried at ambient conditions, then in vacuum. The obtained DT-Au@PS-P2VP nanotubes with AAO membrane were annealed at 140 °C for 120 minutes to produce polymer nanorods with periodic encapsulated holes based on the Rayleigh instability. Then the AAO membranes were dissolved in 5 wt% sodium hydroxide aqueous solution to release the polymer nanorods. After thoroughly cleaned by DI water, these polymer nanorods were re-dispersed in water for ultrasonication. 30 minutes of ultrasonication is enough to cut the DT-Au@PS-P2VP nanorods into short nanoblocks.

The obtained nanoblocks were dispersed in 4.5 ml SDS aqueous solution (the concentration of SDS is 1 mg/ml). A small amount of toluene (0.5 ml) was dropped into this aqueous suspension under sonication. The original clear suspension became opaque gradually. This opaque emulsion was kept at room temperature for 48 hrs to swell the DT-Au@PS-P2VP nanoblocks into particles. After that, the suspension was heated at 70 °C to evaporate toluene, followed by centrifugation at 8000 rpm for 15 minutes to discard the surfactant.

Deposition of Pd nanoparticles to the PS-P2VP shell

DT-Au@PS-P2VP particles (5 mg) were first soaked in $PdCl_2$/HCl/ethanol ($PdCl_2$ 0.1 mM, HCl 1 mM) solution for 10 hours to perform the coordination of metal ions with P2VP groups. Then the composite particles were centrifuged and redispersed in 5 ml H_2O. 0.1 ml of ice cold $NaBH_4$ (10^{-3} M) was used as reducing agent to generate Pd nanoparticels under stirring for 2 min, followed by centrifugation twice at 5000 rpm for 10 min to remove the extra salt in the solution. The amount of Pd decorated on the shell was 17.4 wt.-% according to the TGA measurement.

Catalytic reduction of 4-nitrophenol

Sodium borohydride solution (0.5 ml, 0.1 M) was added to a 4-nitrophenol solution (4.5 ml, 0.11 mM) contained in a glass vessel. The solutions were purged with N_2 to remove oxygen from the system before mixing. A certain amount of Pd@DT-Au@PS-P2VP and DT-Au@PS-P2VP particles (50 μl, 0.36 mg/ml) was added to the mixed solution. UV-vis spectrum was immediately taken every minute in the range of 250 nm to 500 nm.

The apparent constant rate k_{app} can be directly obtained from the curve of $\ln(A/A_0)$ versus time by linear fit. The k_{app} will be proportional to the total surface S of the Pd nanoparticles present in the system: [40]

$$\frac{-dc_t}{dt} = k_{app}c_t = k_1 S c_t$$

where c_t is the concentration of 4-nitrophenol at time t, k_1 is the rate constant normalized to S. The total surface of the Pd nanoparticles, S, was estimated from the TGA results and the nanoparticles size that was obtained from TEM images. For this calculation, the Pd nanoparticles were assumed as spheres and the density of bulk Pd metal was used (ρ = 12.02 g/cm^3).

Characterization

The obtained nanostructures were examined by transmission electron microscopy (TEM) using JEOL JEM-2100 (JEOL GmbH, Eching, Germany). The size distributions of DT-Au cores and polymer shells were measured using Image J software based on their TEM images. More than 100 units were counted. In order to confirm the microphase separation of the PS-P2VP shell, the samples were dispersed in ethanol and placed onto copper grids, then stained with I_2 vapor. For the measurement of UV-vis absorption spectra, the DT-Au@PS-P2VP particles in ethanol were placed in quartz sample cell with a 1.0 cm cell path length. UV-vis spectra (ranged from 300 nm to 900 nm) were recorded by using Lambda 650 spectrometer supplied by Perkin-Elmer at 20 °C with reference spectrum of anhydrous ethanol. TGA measurements were conducted using a Netsch STA409PC LUXX from 25 ˚C to 600 ˚C under a constant argon flow (30 ml/min) with a heating rate of 10K/min.

Results and Discussion

Fabrication and characterization of DT-Au@PS-P2VP core-shell particles

Figure 1 illustrates the morphological evolution of the hybrid materials from DT-Au@PS-P2VP nanotubes to core-shell particles. Figure 1a is the TEM image of the DT-Au@PS-P2VP hybrid nanotube after removal of the AAO membrane before thermal annealing. Two different contrasts can be observed between the outer and inner layer of the nanotube. The outer layer with low contrast is PS-P2VP due to the preferential interaction between the P2VP component and the AAO surface. The inner layer with high contrast is DT-Au aggregation, which contains hydrophobic alky chains on the surface of Au nanoparticles. The hydrophobic DT-Au particles have poor interactions with the hydrophilic surface of the AAO wall, resulting in the phase separation to keep lower surface energy. The bilayered nanotubes confined in AAO channels were then thermally annealed above the glass transition temperature (Tg) of PS-P2VP to induce Rayleigh instability. As shown in Figure 1b, nanorods structure with periodical encapsulated holes are formed after thermal annealing, which is resulted from the undulation of the polymer thin film inside the AAO channels. This result is similar with our previous study on Rayleigh instability of PS-P2VP nanotubes inside AAO channels.[25] The key point here is the location of DT-Au nanoparticles. After thermal annealing, the DT-Au nanoparticles tend to segregate to the edge of the encapsulated holes containing less polymers. This change of location caused by phase separation upon thermal annealing is led by the incompatibility of the PS-P2VP melt with the DT-Au nanoparticles. Lamarre *et al.*[41] have investigated the ligand length effect on the interaction of alkyl-Au nanoparticles with PS-PMMA polymer matrix. According to their work, $C_{18}SH$-capped Au particles are dispersed randomly within PS domains, whereas C_8SH-capped Au particles are relegated to the periphery of them. They attribute this difference to the reduced free volume at the surface of the capping layer. With the decrease of the ligand length, the increase in lateral packing density leads to decreased interaction with the PS chains of the matrix. In our case, DT ($C_{12}SH$) is a rather short ligand compared with the $PS_{50000}P2VP_{16500}$ matrix. Densely packed $C_{12}SH$ ligands can be considered to form a relatively hard organic shell around the Au nanoparticles. Different from long ligand-capped Au nanoparticles which can be considered as soft particles, such hard-sphere like DT-Au

particles have less favorable interaction with the PS-P2VP chains. Thus, the Au nanoparticles tend to be segregated from the polymer matrix.
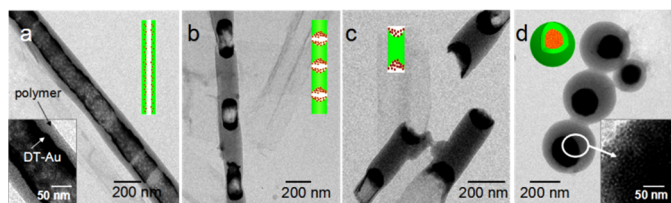
Figure 1. Morphological evolution of core-shell DT-Au@PS-P2VP particles from DT-Au@PS-P2VP hybrid nanotubes. (a) TEM images of DT-Au@PS-P2VP hybrid nanotubes after removal of the AAO membrane. The inset indicates the bilayered distribution of the DT-Au nanoparticles and polymer walls. (b) DT-Au@PS-P2VP nanorods with periodical encapsulated holes. (c) DT-Au@PS-P2VP nanoblocks obtained from ultrasonication of (b). (d) core-shell DT-Au@PS-P2VP particles after swelling of (c). The inset shows the aggregation of small DT-Au nanoparticles in the core part.

Figure 1c shows the broken segments of DT-Au@PS-P2VP, which were obtained from ultrasonication of the hole-containing nanorods for 30 min. Here SDS (1 mg/ml) was added to form a stable aqueous dispersion. From the TEM images, PS-P2VP nanoblocks with DT-Au nanoparticles loaded at both ends (dark region) can be clearly observed. These blocks with a certain amount of DT-Au particles underwent a morphology evolution from anisotropic structure to isotropic core-shell spheres after being swollen by toluene, as shown in Figure 1d. During this swollen procedure, small amount of toluene was added into water under sonication and an oil-water emulsion was formed with SDS as surfactant. The hydrophobic DT-Au nanoparticles tended to be encapsulated by PS-P2VP due to the relatively stronger interactions between P2VP blocks and water (the solubility parameters of P2VP, n-Dodecane and H_2O are 21.7 $MPa^{1/2}$,[42] 16.0 $MPa^{1/2}$ and 48.0 $MPa^{1/2}$,[43] respectively). This adjustment driven by the lowering of interfacial energy results in the aggregation of DT-Au nanoparticles as core (Figure 1d) and PS-P2VP layer as shell. The final evaporation of toluene solidified the core-shell structure of the DT-Au@PS-P2VP particles in aqueous solution.

Moreover, the sizes of the DT-Au nanoparticles before and after the morphology evolution have been studied. Miyake et al[39] reported that DT protected Au nanoparticles underwent a size growing induced by thermal annealing. They showed that annealing at 150 °C for 30 min led Au nanoparticles grow from 1.5 nm to 3.4 nm in diameter. In our experiment, almost no change has been observed for the Au particle size before and after the annealing (Figure S1a and S1b). As shown in Figure S2 in the supporting information, the single Au particle can be clearly distinguished in the final core-shell particles. The aggregated DT-Au nanoparticles are still encapsulated in the polymer phase, which effectively stabilizes the Au nanoparticles and prevents the coherence of the adjacent particles.

Tunable loading of different amounts of DT-Au nanoparticles
Until now, different methods have succeeded in loading metal nanoparticles to polymer nanostructures.[14-21] However, it is still critical to control both the distribution and the loading content

of the metal nanoparticles within the target polymer domains. In our study, the effect of DT-Au content on the morphology of the hybrid particles has been investigated. Figure 2 displays the morphologies of the particles prepared with different amounts of DT-Au keeping the PS-P2VP amount constant (60 mg/ml). When 5 mg/ml of the DT-Au is mixed with the PS-P2VP, a thin layer of DT-Au nanoparticles can be found at the holes of the rod-like segments (Figure 2a). With the increase of DT-Au content, larger aggregations of the DT-Au nanoparticles can be found at the holes of the rod-like structures. When the DT-Au content increases from 5 mg/ml to 20, 30 and 40 mg/ml, the corresponding radius of the DT-Au cores in the final spheres increases from 41 nm to 65, 115 and 180 nm (Figure 2c-h), respectively. As shown in Figure 2h, the DT-Au nanoparticles occupy most space of the polymer spheres, and a very thin layer of polymer shell can be observed. Moreover, at low DT-Au content, the Au cores prefer to distribute near the polymer surface (Figure 2b), while the larger cores prefer to distribute in the center of the particles (Figure 2f, 2h). This may be due to the better mobility of the smaller DT-Au aggregations in polymer droplet, which allows more flexibilities of the spatial distribution. Figure 3 shows the change of the hybrid particles size as a function of the DT-Au content, from which a clearly increasing trend of the core sizes with increased DT-Au content can be observed. Meanwhile, the size of the whole composite particle rarely changed for all samples.
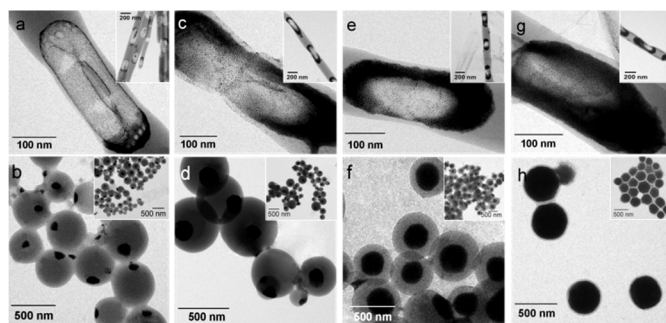
Figure 2. TEM images of DT-Au@PS-P2VP nanostructures with different DT-Au contents. Up panel shows the hybrid nanorods with periodic DT-Au aggregations inside, inset is the image at low magnification. Down panel shows the final core-shell composite particles. $c_{PS-b-P2VP}$ = 60mg/ml, c_{DT-Au} = 5 mg/ml (a, b), 20 mg/ml (c, d), 30 mg/ml (e, f), and 40 mg/ml (g, h), respectively.
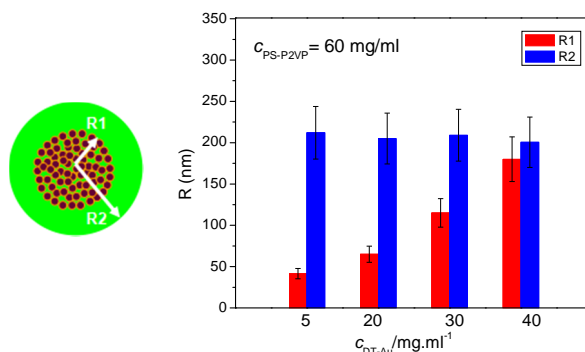
Figure 3. Average radius of DT-Au cores and polymer shells for samples prepared with different amounts of DT-Au nanoparticles.

The influence of the polymer concentration has been also investigated by keeping the DT-Au amount constant (20 mg/ml). As shown in Figure 4 and 5, an increase in the polymer concentration from 40 mg/ml to 60 and 90 mg/ml leads to a decrease in the core radius from 83 nm to 70 and 51nm, respectively. Because the volume of the wetting solution (DT-Au@PS-P2VP) and the quantity of the AAO membranes used in the experiment are the same, nanotubes with thicker walls have been produced at higher concentration of the polymers. During the undulation of the polymer film, smaller amplitude is needed to form the bridge across the AAO channel. Thus, more polymer blocks can be generated, resulting in increasing of total particle number after swollen in the toluene-water emulsion. In this way, the amount of DT-Au particles per nanosphere is reduced, exhibiting smaller core size.
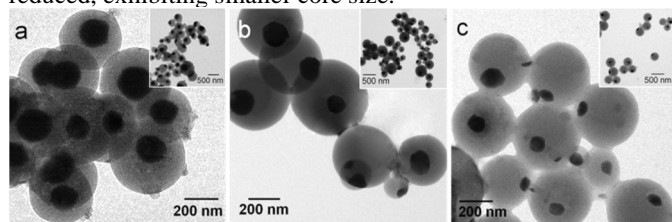
Figure 4. TEM images of the DT-Au@PS-P2VP core-shell particles with different concentrations of polymer but constant concentration of DT-Au (20 mg/ml). $c_{PS-b-P2VP}$ = 40mg/ml (a), 60 mg/ml (b) and 90 mg/ml (c), respectively.
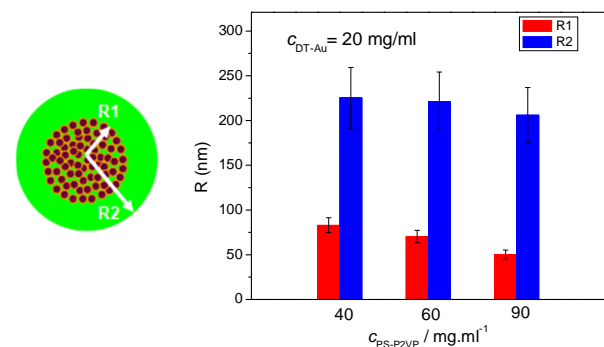
Figure 5. Average radius of DT-Au cores and polymer shells for samples prepared with different amounts of PS-P2VP.

Optical properties of DT-Au@PS-P2VP particles with different core sizes

With the increase of the DT-Au nanoparticles amount, larger aggregations are formed in the core part. This process accompanies with a visible color change of the samples from gray pink to dark brown (Figure S3). The surface plasmon resonance (SPR) absorption of the composite particles with different DT-Au core sizes is shown in Figure 6. Compared with the DT-Au nanoparticles (4.1 nm in diameter) which have the absorption band at 497 nm, a significant broadening and red-shift of the absorption band has been found for the DT-Au@PS-P2VP samples. With the increase of the DT-Au core size from 41nm to 65, 115 and 180 nm in radius, the surface plasmon absorption peak red shifts from 530 nm to 580, 600 and 630 nm, respectively. This is due to the reason that the aggregation of encapsulated Au nanoparticles leads to a decrease in the interparticle spacing, resulting in the occurrence of plasmonic couplings and therefore a red shift in the SPR

peak.[44] Consequently, the plasmon absorption band is at relatively longer wavelengths for larger Au aggregate sizes with closely spaced nanoparticles.[45]

Decoration of the DT-Au@PS-P2VP core-shell particles with Pd nanoparticles

Such core-shell structured DT-Au@PS-P2VP particles are good candidates for spatial organization of a second metal nanoparticles due to the ordered micropahse separation structure of the polymer shell. Without staining of P2VP, no microphase structure can be seen in both PS-P2VP particles (Figure 7a) and core-shell DT-Au@PS-P2VP particles (Figure 7b). After staining with I_2, the ordered microphase separation structure can be obviously observed (spherical, Figure 7c and 7d). This indicates that the introduction of DT-Au nanoparticles into polymer solution has no influence on the microphase separation of PS-P2VP. Because the PS-P2VP shell contains pyridine units, various types of metal precursors (i.e. $HPt_2Cl_6·6H_2O$, $AgNO_3$ and H_2PtCl_4) can be coordinated with them, which leads to the assembly of a second metal nanoparticles by an in situ reduction process. As shown in Figure 7e, Pd nanoparticles with diameter of 3 nm have been selectively distributed in the P2VP domains. The regular spaces between the adjacent Pd domains should be the PS phase. As a result, the DT-Au aggregations and ordered Pd nanoparticles were selectively assembled at the core part and the shell part of the composite particles, respectively. Moreover, no shift was found in the UV-Vis spectra after Pd deposition (Figure S4), indicating that further loading of Pd nanoparticles did not affect the characteristic absorption of the DT-Au@PS-P2VP particles.
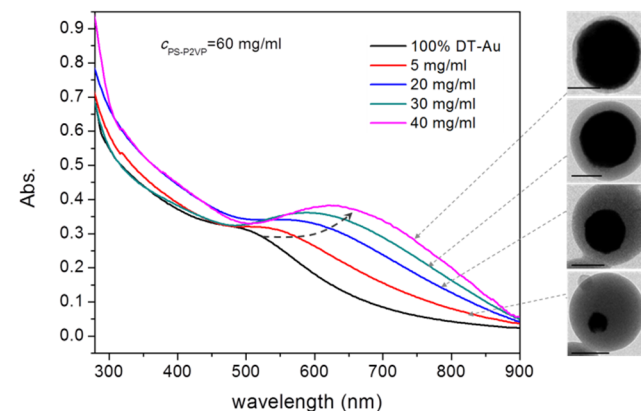
Figure 6. UV-vis spectra of the samples with constant amount of polymer but different amount of DT-Au nanoparticles. Scale bar in TEM images: 200 nm.
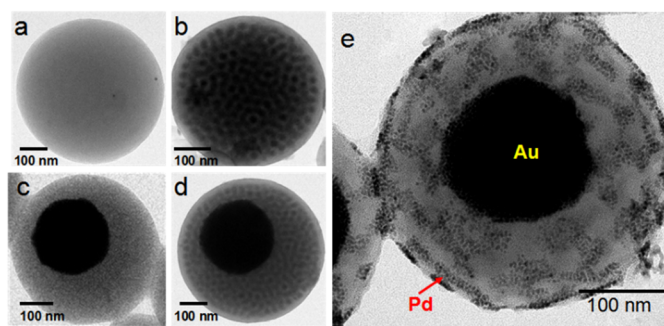
Figure 7. TEM images of the PS-P2VP (a, b) and DT-Au@PS-P2VP (c, d) particles before (a, c) and after (b, d) staining. The

darker dots are P2VP domains which are stained with I$_2$ vapor. (e) Pd decorated core-shell DT-Au@PS-P2VP spheres.

Catalytic activity of the Pd@DT-Au@PS-P2VP particles

Pd nanoparticles are well-known to be catalytically active for reduction or coupling reactions.[40,46] In our study, the obtained Pd@DT-Au@PS-P2VP particles are further used as catalyst for the reduction of 4-nitrophenol by sodium borohydride.[47-49] Figure 8 shows the UV-vis spectrum and kinetic analysis of the reduction of 4-nitrophenol. When Pd@DT-Au@PS-P2VP particles are used as catalyst, the characteristic absorption at 400 nm reduces with time due to the conversion of 4-nitrophenol. Another characteristic absorption at 300 nm appears and increases with time due to the generation of the end product, aminophenol (Figure 8a). In order to test which metal particle in the Pd@DT-Au@PS-P2VP composite particles really contributes to the catalysis, the DT-Au@PS-P2VP particles have been also used as control catalyst. In this case, no catalytic effect is found in the experimental time range (Figure 8b), which demonstrates that the catalytic capability of the Pd@DT-Au@PS-P2VP particles arises only from the Pd nanoparticles. This is because that the DT-Au aggregations are encapsulated in the polymer shell, which blocks the diffusion of 4-nitrophenol to the metal surface. In addition, the DT ligands capped on the Au nanoparticles will also hinder the active site and weaken the catalytic activity. The reduction of 4-nitrophenol follows a pseudo-first order kinetic due to the excess of borohydride. As shown in Figure 8c, a linear dependence of ln(A/A$_0$) on the reaction time can be observed when using Pd@DT-Au@PS-P2VP particles as the catalyst. The slope of this linear section leads to the apparent reaction rate (k_{app}), which is 1.72×10^{-3} s^{-1}.
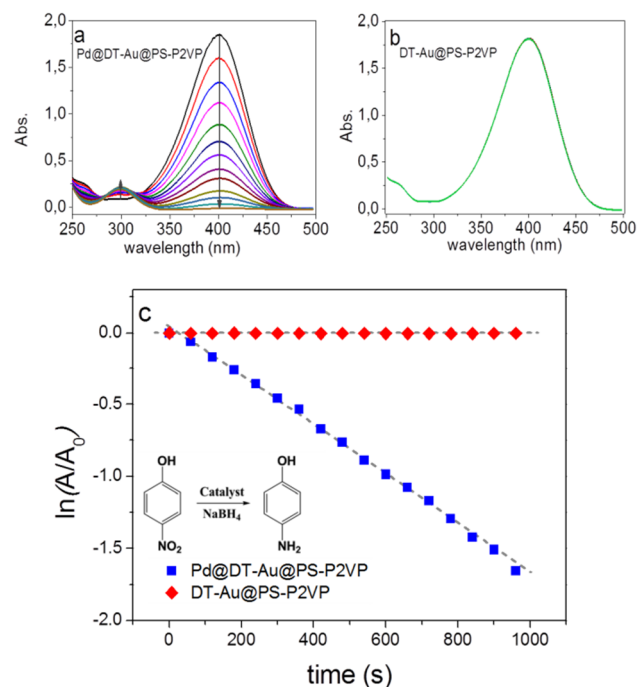
Figure 8. UV-vis spectrum of the reduction of 4-nitrophenol using Pd@DT-Au@PS-P2VP (a) and DT-Au@PS-P2VP (b) as catalyst. (c) Kinetic analysis of the reaction with Pd@DT-Au@PS-P2VP (squares) and DT-Au@PS-P2VP (diamonds) as catalysts.

Table 1 summarizes the catalytic activity of some reported Pd nanocatalysts with similar size for the reduction of 4-nitrophenol. Here the surface area-normalized rate constant, k$_1$, is applied for direct comparison.[47] In general, the Pd@DT-Au@PS-P2VP composite particles show quite high catalytic activity compared to other reported systems. For example, it is higher than that of peptide, protein and PAMAM dendrimer stabilized Pd nanocatalyst systems. In addition, it is found that for the metal nanoparticles with similar size, the carrier system can have a strong influence on the rate constant of the immobilized nanoparticles. The present PS-P2VP block copolymer nanospheres and polymeric brushes act as efficient carrier systems for the immobilization of catalytic active Pd nanoparticles.

Table 1. Catalytic activity of the metal nanoparticles for the reduction of 4-nitrophenol.

Sample	Carrier system	Metal	d^a (nm)	T [°C]	k_1^b (s^{-1}m^{-2}l)
Pd@DT-Au@PS-P2VP (present study)	DT-Au@PS-P2VP	Pd	3.1±0.2	20	0.08
Yuan 2012 [48]	PS-poly(ionic liquid) brushes	Pd	2.1±0.2	20	0.58
Mei 2007 [52]	Spherical polyelectrolyte brushes	Pd	2.4±0.5	15	1.1
Esumi 2004 [53]	PAMAM dendrimer	Pd	1.8±0.4	15	0.003
Behrens 2009 [54]	Protein	Pd	2.8±0.5	22	0.048
Bhandari 2011 [55]	Peptide	Pd	2.6±0.5	20	0.017

[a] d: Diameter of the metal nanoparticles
[b] k_1: Rate constant normalized to the surface area of the particles in the system

Conclusion

In this study, we demonstrate a novel route to assemble two types of metal nanoparticles onto block copolymer nanospheres with ordered spatial distribution. DT-Au@PS-P2VP core-shell particles are first fabricated by swelling the short polymer rods containing periodic DT-Au aggregations, which are derived from Rayleigh instability of bilayered DT-Au@PS-P2VP nanotubes confined in AAO cylindrical pores. By using different amount of DT-Au nanoparticles, the core size can be adjusted directly. Moreover, the composite particles with larger DT-Au cores exhibit a red shift of the surface plasmon absorption band in the UV-Vis spectrum. Because the PS-P2VP shell has highly ordered microphase separation structure, a second metal, Pd nanoparticles, have been successfully coated on the shell with patterned distribution, which can work efficiently as catalyst for the reduction of 4-nitrophenol. This study not only provides an effective approach for the sufficient location of different metal nanoparticles into polymer particles, but also demonstrates the functionalization of the polymer particles with optical and catalytic properties derived from two different metal nanoparticles, respectively. The assembly of other types of metal nanoparticles and the optimized properties of the resultant composite particles will be studied in the future. Such multi-component nanomaterials will have potential

applications in high-performance catalysis, bioengineering and medical therapy.

Acknowledgements

Notes and references

Soft Matter and Functional Materials, Helmholtz-Zentrum Berlin für Materialien und Energie, Hahn-Meitner Platz 1, 14109 Berlin, Germany Email address: yan.lu@helmholtz-berlin.de

1   K. H. Ku, J. M. Shin, M. P. Kim, C. Lee, M. Seo, G. Yi, S. G. Jang, and B. J. Kim, *J. Am. Chem. Soc.,* 2014, **136**, 9982.

2   W. Li, S. Liu, R. Deng, J. Wang, Z. Nie, and J. Zhu, *Macromolecules*, 2013, **46**, 2282.

3   S. G. Jang, E. J. Kramer, C. J. Hawker, *J. Am. Chem. Soc.,* 2011, **133**, 16986.

4   A. Halevi, S. Halivni, M. Oded, Axel H. E. Müller, U. Banin, R. Shenhar, *Macromolecules,* 2014, **47**, 3022.

5   C. H. Braun, T. V. Richter, F. Schacher, Axel H. E. Müller, E. J. W. Crossland, S. Ludwigs, *Macromol. Rapid Commun*., 2010, **31**, 729.

6   A. H. Gröschel, A. Walther, T. I. Löbling, F. H. Schacher, H. Schmalz, A. H. E. Müller, *Nature*, 2013, **503**, 247.

7   R. Deng, S. Liu, F. Liang, K. Wang, J. Zhu, and Z. Yang, *Macromolecules,* 2014, **47**, 3701.

8   Z. H. Nie, A. Petukhova, E. Kumacheva, *Nat. Nanotechnol.,* 2010, **5**, 15.

9   S. C. Warren, F. J. DiSalvo, U. Wiesner, *Nat. Mater.,* 2007, **6**, 156.

10 K. Liu, A. Ahmed, L. Chung, K. Sugikawa, G. Wu, Z. Nie, G. Gordon, E. Kumacheva, *ACS Nano,* 2013, **7**, 5901.

11 Y. Zhu, L. Fan, B. Yang, and J. Du, *ACS Nano*, 2014, **8**, 5022.

12 Y. Lin, V. K. Daga, E. R. Anderson, S. P. Gido, J. J. Watkins, *J. Am. Chem. Soc.,* 2011, **133**, 6513.

18 G. Chen,Y. Wang, M. Yang, J. Xu, S. J. Goh, M. Pan, H. Chen, *J. Am. Chem. Soc.,* 2010, **132**, 3644.

14 Y. Mai,A. Eisenberg, *J. Am. Chem. Soc.,* 2010, **132**, 10078.

15 H. Yabu, T. Jinno, K. Koike, T. Higuchi, M. Shimomura, *J. Polym. Sci. Pol. Phys.,* 2011, **49**, 1717.

16 H. Yabu, K. Koike, K. Motoyoshi, T. Higuchi, M. Shimomura, *Macromol. Rapid Commun.,* 2010, **31**, 1267.

17 J. Zhu, R. C. Hayward, *J. Am. Chem. Soc.,* 2008, **130**, 7496.

18 H. Y. Chen, S. Abraham, J. Mendenhall, S. C. Delamarre, K. Smith, I. Kim, C. A. Batt, *ChemPhysChem,* 2008, **9**, 388.

19 W. Li, S. Liu, R. Deng, J.Zhu, *Angew. Chem., Int. Ed.,* 2011, **50**, 5865.

20 M. P. Kim, K. H. Ku, H. J. Kim, S. G. Jang, G. R. Yi, and B. J. Kim, *Chem. Mater.,* 2013, **25**, 4416.

21 L. Wang, S. L. Mei and Z. X. Jin, *Macromol. Chem. Phys.,* 2013, **214**, 2579.

22 S. G. Jang, D. J. Audus, D. Klinger, D. V. Krogstad, B. J. Kim, A. Cameron, S. W. Kim, K. T. Delaney, S. M. Hur, K. L. K., G. H. Fredrickson, E. J. Kramer, and C. J. Hawker, *J. Am. Chem. Soc.,* 2013, **135**, 6649.

23 H. Yabu, T. Jinno, K. Koike, T. Higuchi, and M. Shimomura, *Macromolecules,* 2011, **44**, 5868.

24 R. Liang, J. P. Xu, R. H. Deng, K. Wang, S. Q. Liu, J. Y. Li, and J. T. Zhu, *ACS Macro Lett.,* 2014, **3**, 486.

25 S. L. Mei, X. D. Feng, and Z. X. Jin, *Macromolecules*, 2011, **44**, 1615.

26 X. D. Feng and Z. X. Jin, *Macromolecules,* 2009, **42**, 569.

27 C. R. Martin, *Chem. Mater.,* 1996, **8**, 1739.

28 S. Ai, G. Lu, Q. He, J. Li, *J. Am. Chem. Soc.,* 2003, **125**, 11140.

29 G. A. O'Brien, A. J. Quinn, D. A. Tanner, G. Redmond, *Adv. Mater.,* 2006, **18**, 2379.

30 M. Steinhart, R. B. Wehrspohn, U. Gosele, J. H. Wendorff, *Angew. Chem., Int. Ed.,* 2004, **43**, 1334.

31 S. I. Moon, T. J. McCarthy, *Macromolecules,* 2003, **36**, 4253.

32 M. Steinhart, J. H. Wendorff, A. Greiner, R. B. Wehrspohn, K. Nielsch, J. Schilling, J. Choi, U. Gosele, *Science,* 2002, **296**, 1997.

33 L. Rayleigh, *Proc. London Math. Soc.,* 1878, **10**, 4.

34 J. T. Chen, M. Zhang, T. P. Russell, *Nano Lett.,* 2007, **7**, 183.

35 D. Chen, J. T. Chen, E. Glogowski, T. Emrick, T. P. Russell, *Macromol. Rapid Commun.,* 2009, **30**, 377.

36 B. Wiley, Y. Sun, Y. Xia, *Acc. Chem. Res.,* 2007, **40**, 1067.

37 M. C. Daniel, D. Astruc, *Chem. Rev.,* 2004, **104**, 293.

38 M. B. Cortie, A. M. McDonagh, *Chem. Rev.,* 2011, **111**, 3713.

39 T. Teranishi, S. Hasegawa, T. Shimizu and M. Miyake, *Adv. Mater.,* 2001, **13**, 1699.

40 P. Hervés, M. Pérez-Lorenzo, L. M. Liz-Marzán, J. Dzubiella, Y. Lu, M. Ballauff, *Chem. Soc. Rev.*, 2012, **41**, 5577.

41 S. S. Lamarre, C. Lemay, C. Labrecque, and A. M. Ritcey, *Langmuir,* 2013, **29**, 10891.

42 K. Kulbaba, M. J. MacLachlan, C. E. B. Evans, I. Manners, *Macromol. Chem. Phys.,* 2001, **202**, 1768.

43 Barton, *Handbook of Solubility Parameters, CRC Press*, 1983.

44 P. K. Jain, W. Huang, M. A. El-Sayed, *Nano Lett.,* 2007, **7**, 2080.

45 A. A. Lazarides, G. C. Schatz, *J. Phys. Chem. B,* 2000, **104**, 460.

46 M. R. Hartings, *Nat. Chem.,* 2012, **4**, 764.

47 S. Wu, J. Dzubiella, J. Kaiser, M. Drechsler, X. Guo, M. Ballauff, Y. Lu, *Angew. Chem. Int. Ed.,* 2012, **51**, 2229.

48 J. Yuan, S. Wunder, F. Warmuth, Y. Lu, *Polymer,* 2012, **53**, 43.

49 S. Gu, S. Wunder, Y. Lu, M. Ballauff, R. Fenger, K. Rademann, B. Jaquet, A. Zaccone, *J. Phys. Chem. C,* 2014, **118**, 18618.

50 R. He, Y.C. Wang, X. Y.Wang, Z. Wang, G. Liu, W. Zou, L. Wen, Q. Li, X. P. Wang, X. Chen, J. Zeng, J.G. Hou, *Nat. Comm.*, 2014, **5**, 4327.

51 J. Zeng, Q. Zhang, J. Chen and Y. Xia, *Nano Lett.,* 2010, **10**, 30.

52 Y. Mei, Y. Lu, F. Polze, M. Ballauff, M. Drechsler, *Chem. Mater.*, 2007, **19**, 1062.

53 K. Esumi, R. Isono, T. Yoshimura, *Langmuir*, 2004, **20**, 237.

54 S. Behrens, A. Heyman, R. Maul, S. Essig, S. Steigerwald, A. Quintilla, et al. *Adv. Mater.*, 2009, **21**, 3515.

55 R. Bhandari, R. Bhandari, MR Knecht, *ACS Catal.*, 2011, **1**, 89.

Journal of Materials Chemistry A Accepted Manuscript

The table of contents

Pd@PS-P2VP @DT-Au core-shell particles are fabricated based on the modified AAO template method and an in situ reduction process, showing efficient optical and catalytic properties.

S. Mei, J. Cao, and Y. Lu*

Title: Controllable Assembly of Two Types of Metal Nanoparticles onto Block Copolymer Nanospheres with Ordered Spatial Distribution

ToC figure